Journal of Catalysis **185,** 487–495 (1999)
Article ID jcat.1999.2504, available online at http://www.idealibrary.com on IDEAL®

Orientation of MoS_2 Clusters Supported on Two Kinds of γ-Al_2O_3 Single Crystal Surfaces with Different Indices

Y. Sakashita and T. Yoneda

Advanced Catalysts Research Laboratory, Petroleum Energy Center, KSP D-1237, 3-2-1, Sakado, Takatsu, Kawasaki, Kanagawa 213, Japan

Received January 12, 1999; revised March 22, 1999; accepted March 24, 1999

The effect of surface orientations of supports on microstructures of MoS_2 clusters was investigated by high-resolution electron microscopy observations of Mo model catalysts supported on γ-Al_2O_3 single crystal thin films with two kinds of surface orientations. By use of an electron beam evaporation method, epitaxial γ-Al_2O_3 single crystal thin films with smooth surfaces were successfully grown on (111) and (100) $MgAl_2O_4$ substrates. Mo model catalysts were prepared on these γ-Al_2O_3 thin films by the vacuum evaporation method, using MoO_3 as a source material. After sulfidation at 773 K, relatively uniform basal bonded clusters were grown on (111) γ-Al_2O_3 thin films. The particle size distribution was relatively narrow because of some cluster–support interaction. Their mean particle size was approximately 1.73 nm. On the other hand, edge bonded clusters were grown on (100) γ-Al_2O_3 thin films. The mean cluster length was approximately 2 nm. From further discussions on the cluster–support interface at an atomic level, it seems reasonable to conclude that important factors for determining the orientation of MoS_2 clusters on γ-Al_2O_3 supports could include similarities between the arrangement of Mo atoms in MoS_2 and the arrangement of Al or O atoms in γ-Al_2O_3 surface.

Key Words: **model catalysts; molybdenum sulfide catalysts; γ-Al_2O_3 single crystal thin films; HREM observation.**

INTRODUCTION

Numerous attempts to clarify the relationships between microstructures of MoS_2 clusters and their catalytic functions in MoS_2-based catalyst systems have been made for a long time because of its important use in several kinds of reactions in refineries, such as hydrogenation, hydrodesulfurization (HDS) and hydrodenitrogenation (HDN), and several models have been proposed (1–4). To take one example, according to the rim–edge model proposed by Daage *et al.*, the hydrogenation pathway occurs on rim sites only, while the HDS pathway occurs on both rim and edge sites (5, 6). However, the structure–function relations are not fully understood due to the difficulties in creating uniform activity sites and evaluating intrinsic activities because of a porous structure associated with the conventional catalysts. Therefore, several kinds of fundamental studies using model catalysts have been performed. Although several metal single crystals, such as molybdenum and nickel, have been generally used as model catalysts (7–9), these kinds of model catalysts without support have a critical disadvantage, which is the differences in the structure of active sites between the model catalysts and real catalysts. In order to avoid this disadvantage, several studies using flat oxide thin films as model supports have been reported (10–15). However, due to their amorphous or polycrystalline structure, uniform clusters with well-controlled active sites have not been prepared yet. By using oxide single crystal substrates as model supports, the authors have tried to prepare well-controlled MoS_2 clusters (16). In the present paper, we describe high-resolution electron microscopy (HREM) observations of Mo model catalysts supported on γ-Al_2O_3 single crystal thin films with two kinds of surface orientations in order to clarify the effect of surface orientations of supports on microstructures of MoS_2 clusters.

EXPERIMENTAL

Preparation and Characterization of γ-Al_2O_3 Thin Films

Since γ-Al_2O_3 has a lot of vacancies in cation positions, it is difficult to obtain γ-Al_2O_3 bulk single crystals large-enough for the experiment. Therefore, we had to prepare γ-Al_2O_3 single crystals in thin film form as the first step. The substrates used for this study were $10 \times 10 \times 0.5$ mm polished spinel ($MgAl_2O_4$) single crystals with surface orientations of (111) and (100). According to the JCPDS 21-1152, $MgAl_2O_4$ has the same spinel type structure as γ-Al_2O_3 and the lattice constant of $MgAl_2O_4$ is 0.808 nm, which is quite close to that of γ-Al_2O_3, 0.7924 nm. The lattice misfit is approximately -2.0%. Consequently, γ-Al_2O_3 thin films are expected to be epitaxially grown on $MgAl_2O_4$ single crystal substrates.

γ-Al_2O_3 thin films were prepared using the electron beam evaporation method. The source material was an α-Al_2O_3 tablet with 99.99% purity. The substrate temperature was kept at 1073 K during deposition. The oxygen gas (99.99% purity) flow rate was 0.1 ml/min, keeping pressure at 1.3×10^{-3} Pa. The deposition time was 5 min, and the

0012-9517/99 $30.00

film thickness was about 5 nm measured by a quartz oscillator.

The synthesized films were investigated using HREM and atomic force microscopy (AFM). The specimens for HREM observation were prepared using punching, grinding and ion-milling techniques. A Topcon EM-002B was used for HREM analysis and operated at 200 kV with a point resolution of 0.19 nm. A Digital Instruments Nano Scope IIIa was used for AFM analysis and operated in tapping mode. The compositional analyses were carried out using X-ray photoelectron spectroscopy (VG ESCALAB 220i) equipped with a Mg anode and operated at 12 kV and 34 mA. Narrow scans were performed of the O(1*s*), Al(2*p*), and Mg(2*p*) regions at 30 eV pass energy.

Preparation and Characterization of Mo Model Catalysts

MoO_x deposits were prepared on the above-mentioned γ-Al_2O_3 thin films by the vacuum evaporation method using MoO_3 as a source material heated at 783 K in a Knudsen cell. The substrate temperature was kept at 373 K during deposition. In this experimental condition, 3 min deposition prepared 0.3-nm-thick MoO_x as measured by the quartz oscillator. After 30 min oxidation (O_2 atmosphere, 1.3×10^{-3} Pa, 673 K), these deposits were sulfided in 5% H_2S/H_2 at 100 Pa at 573 and 773 K for 30 min, respectively. These Mo model catalysts were investigated using the above-mentioned HREM technique. The compositional analyses of Mo model catalysts before and after sulfidation were carried out using the above-mentioned XPS instrument. Narrow scans were performed of the Mo(3*d*), S(2*p*), O(1*s*), and Al(2*p*) regions at 30 eV pass energy.

RESULTS AND DISCUSSION

Surface Structures of γ-Al_2O_3

As a beginning, ideal surface structures of γ-Al_2O_3 are briefly described in this section for the sake of understanding the below-mentioned discussion concerning the cluster–support interface, although they can be easily found in numerous publications (17, 18). γ-Al_2O_3 group materials, such as γ-Al_2O_3 and η-Al_2O_3, are transition phases derived from dehydration of alumina hydroxide, such as boehmite and bayerite, and have a spinel ($MgAl_2O_4$) type structure. According to the JCPDS 21-1152, $MgAl_2O_4$ has a space group of F*d*3*m* and a cubic system with a lattice constant of 0.808 nm. The distinction between γ-Al_2O_3 and η-Al_2O_3 is usually established by analysis of XRD spectra; γ-Al_2O_3 is defined as a material which has some branches with (400) and (440), while η-Al_2O_3 has no such branches. γ-Al_2O_3 has a tetragonal system with lattice constants of $a = 0.801$ nm and $c = 0.773$ nm. On the other hand, η-Al_2O_3 has a cubic system with a lattice constant of 0.792 nm. In this paper, however, the term "γ-Al_2O_3" represents γ-Al_2O_3 group materials.

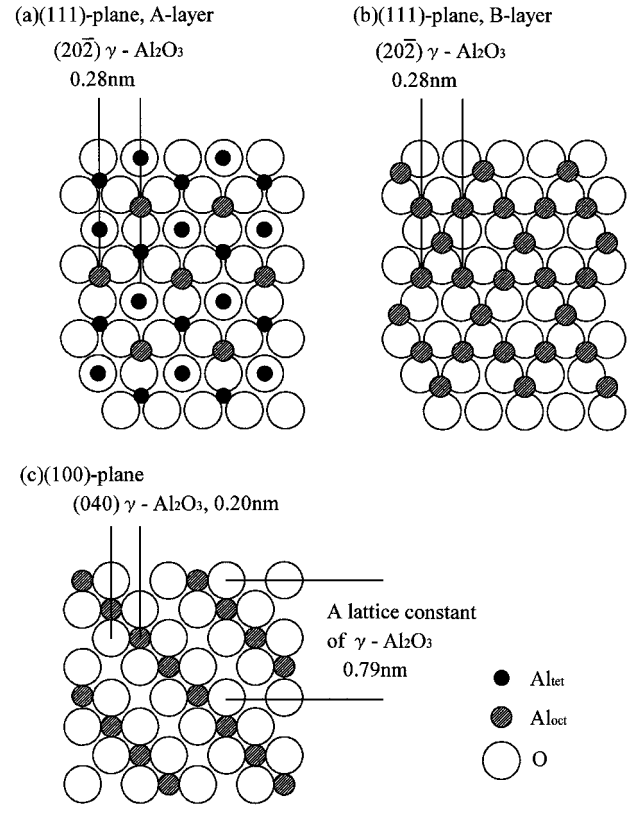

FIG. 1. Surface structures of the alumina spinel lattice: (a) (111) plane, A-layer, (b) (111) plane, B-layer, (c) (100) plane. Al_{tet} and Al_{oct} mean Al atoms located in tetrahedral and octahedral cation positions, respectively.

The unit cell of γ-Al_2O_3 consists of 32 oxygen atoms and $21\frac{1}{3}$ aluminum atoms, hence, $2\frac{2}{3}$vacant cation positions occur in one unit cell. The oxygen lattice is built up by a cubic close-packed stacking of oxygen layers.

In the alumina spinel lattice parallel to the (111) plane, there are two types of layers containing two different cation distributions, which are generally called A- and B-layers. As shown in Figs. 1a and 1b, the B-layer contains only octahedral cation positions, while the A-layer contains both tetrahedral and octahedral cation positions. For energetic reasons, a crystallite is usually considered to be terminated by anion layers. In the case of (111) γ-Al_2O_3, the surface layer should be the cubic close-packed oxygen layer.

Similarly, two cation arrangements are present in the alumina spinel lattice parallel to the (100) plane. One layer consists of a square lattice of oxygen atoms and only octahedral cation positions shown in Fig. 1c, while the other consists of only tetrahedral cation positions.

Surface Structures of MoS_2

Next, ideal surface structures of MoS_2 are also described briefly here (2, 10). Bulk MoS_2 generally has a hexagonal

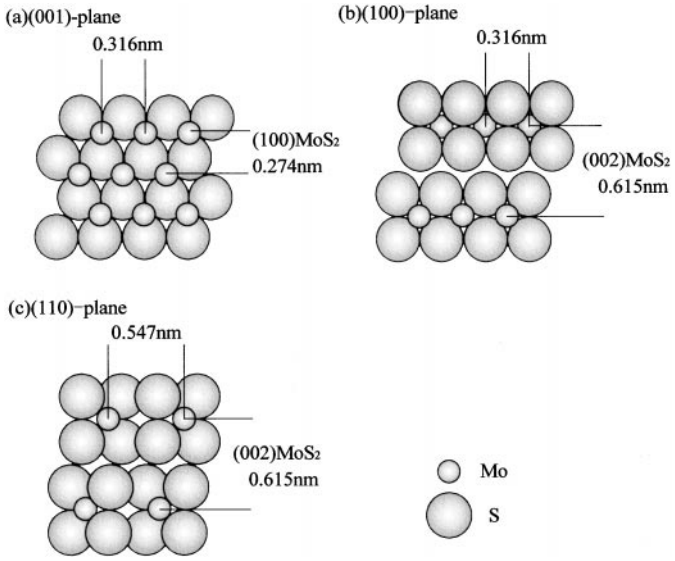

FIG. 2. Surface structures of the bulk MoS_2 lattice with low Miller indices: (a) (001) plane, (b) (100) plane, (c) (110) plane.

system with lattice constants of $a = 0.3160$ nm and $c = 1.2295$ nm according to the JCPDS 6-0097. In this system, each Mo layer is sandwiched between two S layers. A Mo atom is located in the center of a S triangular prism and present in the 4+ state. Each S atom has three bonds to Mo atoms and completely filled $3s^2 3p^6$ octets. Consequently, a S–S interaction between two S–Mo–S layers caused by van der Waals force is very weak. S–Mo–S layers are stacked along the *c*-axis, but easily cleave parallel to S–Mo–S layers.

This S–Mo–S layered structure leads to two major types of exposed surface planes, which are generally called the basal plane and the edge plane. The basal plane, namely the (001) plane, is parallel to the S–Mo–S layers as shown in Fig. 2a. For energetic reasons, the basal plane is usually terminated by a close-packed S layer. Therefore, the basal plane is generally accepted to be non-active for catalytic reactions. On the contrary, the edge plane, which is perpendicular to the S–Mo–S layer, possesses coordinately unsaturated Mo atoms. There are two typical edge planes, which are the (100) plane as shown in Fig. 2b and the (110) plane as shown in Fig. 2c. In case of the (110) plane, four Mo atoms in Fig. 2c are present in the same plane, namely, a surface plane. In case of the (100) plane, however, six Mo atoms in Fig. 2b are not present in the same plane. For energetic reasons, it is well-known that the (100) plane is more stable than the (110) plane. Accordingly, MoS_2 particles generally tend to have hexagonal crystal habits. Anyhow, the important point to note is that both edge planes, the (100) plane and the (110) plane, possess coordinately unsaturated Mo atoms which are believed to be active sites for catalytic reactions.

Characterization of γ-Al_2O_3 Thin Films

The TEM micrographs of the γ-Al_2O_3 thin film deposited on the (111) $MgAl_2O_4$ substrate have no characteristic feature, such as visible particles and islands. By increasing the magnification of the micrograph as shown in Fig. 3a, we can clearly see the structure image. Interplanar spacings along [110] directions calculated from this image are approximately 0.28 nm, which agree with that of (220) γ-Al_2O_3, 0.280 nm. The selected-area diffraction pattern as shown in Fig. 3b indicates that the synthesized thin film has a single crystal structure and agrees with the characteristic pattern of (111) γ-Al_2O_3. From the HREM observation, it is clearly found that γ-Al_2O_3 thin film was epitaxially grown on (111) $MgAl_2O_4$ substrate. Almost the same results were obtained in the case of the (100) $MgAl_2O_4$ substrate.

Figure 4a shows the surface morphology of the γ-Al_2O_3 thin film deposited on the (100) $MgAl_2O_4$ substrate

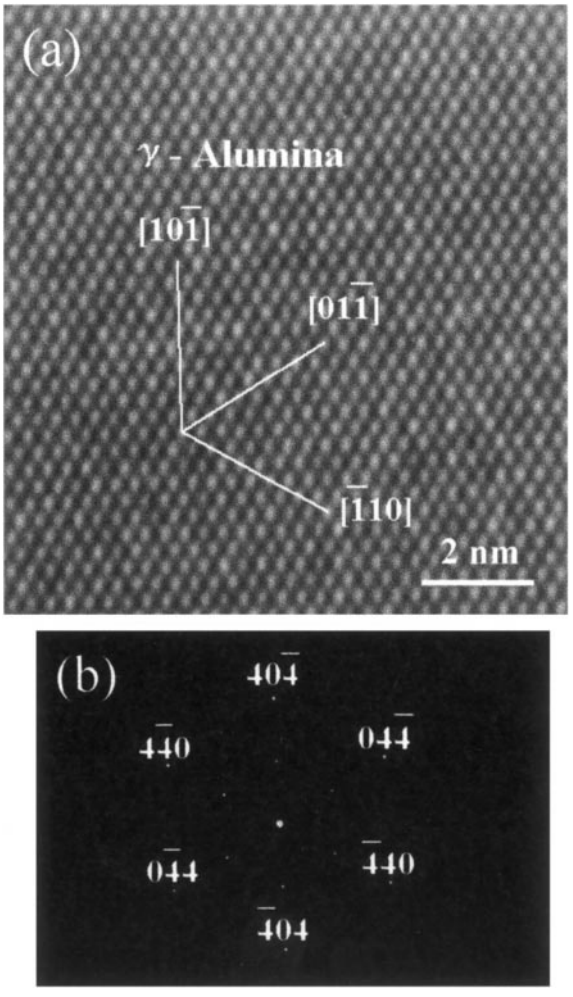

FIG. 3. (a) HREM image of the γ-Al_2O_3 thin film deposited on the (111) $MgAl_2O_4$ substrate. (b) Selected-area diffraction pattern of the γ-Al_2O_3 thin film.

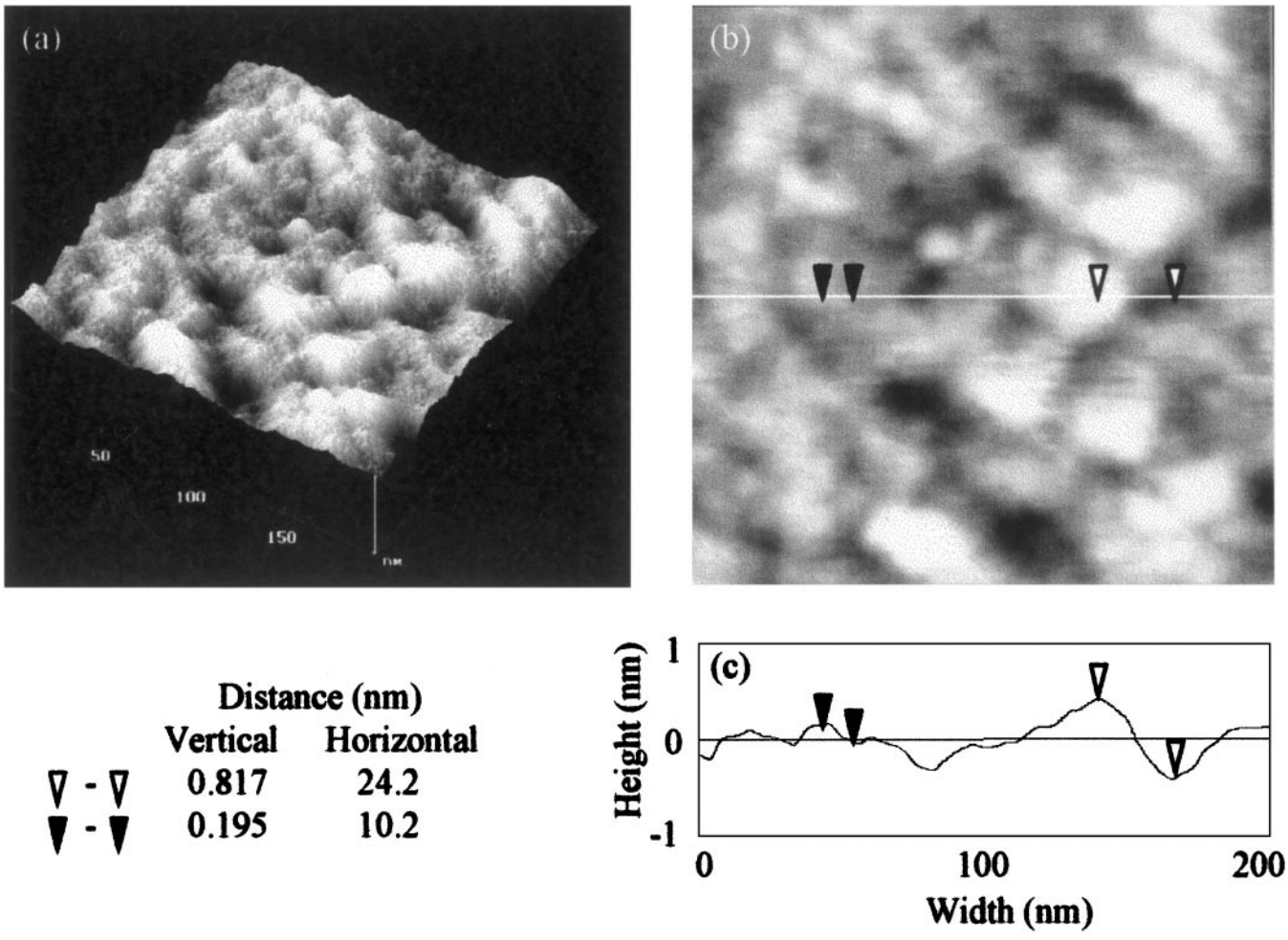

FIG. 4. Surface morphology of the γ-Al_2O_3 thin film deposited on the (100) $MgAl_2O_4$ substrate measured by AFM. (a) Bird's-eye view, (b) top view, (c) cross-sectional profile.

measured by AFM. The scanning area is 200×200 nm. Figure 4c shows the cross-sectional profile along the white line shown in Fig. 4b. The vertical distance between white triangular markers is approximately 0.82 nm, which is almost equal to the lattice constant of γ-Al_2O_3, 0.79 nm. In addition, the vertical distance between black triangular markers is approximately 0.20 nm, in agreement with a quarter of the lattice constant of γ-Al_2O_3. Therefore, the synthesized film has a very smooth surface with a lattice constant level.

The compositions of both γ-Al_2O_3 thin films measured by XPS were shown in Table 1. The O : Al atomic ratio were almost consistent with the 1.5 stoichiometry of bulk alumina and the amounts of Mg were negligible. These results indicate the $MgAl_2O_4$ substrates were uniformly covered with γ-Al_2O_3 thin films.

TABLE 1

Compositions of γ-Al_2O_3 Thin Films and Mo Model Catalysts by XPS Analysis

	(100)					(111)				
Orientation of γ-Al_2O_3	%Mo	%S	%O	%Al	%Mg	%Mo	%S	%O	%Al	%Mg
γ-Al_2O_3 thin films	—	—	62.9	35.7	1.4	—	—	60.5	38.2	1.3
Before sulfidation	6.4	—	63.2	30.4	—	5.6	—	62.5	31.9	—
Sulfidation at 573 K	6.4	7.9	52.7	33.0	—	5.2	6.4	53.7	34.7	—
Sulfidation at 723 K	6.3	16.5	43.0	34.2	—	5.3	14.1	47.3	33.3	—

Judging from the foregoing results, such as the TEM, AFM, and XPS analysis, it is obvious that epitaxial γ-Al_2O_3 single crystal thin films with atomically smooth surfaces were successfully grown on (100) and (111) $MgAl_2O_4$ substrates using the electron beam evaporation method. The epitaxial relations were (100) γ-Al_2O_3//(100) $MgAl_2O_4$, [010] γ-Al_2O_3//[010] $MgAl_2O_4$ and (111) γ-Al_2O_3//(111) $MgAl_2O_4$, [101] γ-Al_2O_3//[101] $MgAl_2O_4$, respectively.

HREM Observation of Mo Model Catalysts Supported on γ-Al_2O_3/(111) $MgAl_2O_4$ Substrates

The TEM micrographs of the Mo model catalyst supported on the γ-Al_2O_3/(111) $MgAl_2O_4$ substrate after MoO_x deposition and oxidation at 673 K have no apparent differences compared with those before deposition, as shown in Fig. 3. Considering our XPS results shown in Table 1, which indicate nonnegligible amounts of Mo were deposited on the thin film, we think this HREM observation suggests that MoO_x could be present in highly dispersed form or as amorphous particles.

The TEM micrograph of the Mo model catalyst supported on the γ-Al_2O_3/(111) $MgAl_2O_4$ substrate after sulfidation at 573 K has no visible particles. By increasing the magnification of the micrograph as shown in Fig. 5a, we can see only the atomic image of the substrate, which is almost the same as Fig. 3a. This indicates that MoO_xS_y could be grown in highly dispersed form or as amorphous particles.

Figure 6a shows the TEM micrograph of the Mo model catalyst supported on the γ-Al_2O_3/(111) $MgAl_2O_4$ substrate after sulfidation at 773 K. Many small particles are visible. Figure 6b shows representative particles by increasing the magnification of the micrograph. It indicates lattice images of the particle and alumina film, which meet at a 30° angle. The interplanar spacing of the particle is approximately 0.25 nm. Most of the particles have the same geometrical features. The selected-area diffraction pattern shown in Fig. 6c indicates that new spots indicated by white arrows appear in the characteristic pattern of (111) γ-Al_2O_3. The interplanar spacing calculated from these new spots is approximately 0.25 nm, in agreement with that of the above-mentioned particles. Consequently, these new spots could be derived from the particles.

Here, the cluster–support interface of this Mo model catalyst will be discussed, following the example of the (110) plane proposed by Schuit *et al*. (17). There are two possibilities. One is an altered A-layer, the other is an altered B-layer. Since a surface layer of (111) γ-Al_2O_3 should be a cubic close-packed oxygen layer as mentioned above, it seems reasonable to suppose that Mo atoms are located in the cation positions on the oxygen layer where Al atoms in the next layer should be located. Consequently, we tried to exchange all Al atoms in both A- and B-layers of (111) γ-Al_2O_3 by Mo atoms, as shown in Figs. 7a and 7b, respectively. In both cases, the arrangements of Mo atoms which have six symmetry axes are similar to that in Fig. 2a. The epitaxial relations are (001)MoS_2//(111) γ-Al_2O_3, [100]MoS_2//[101] γ-Al_2O_3 in the altered A-layer and (001)MoS_2//(111) γ-Al_2O_3, [110]MoS_2//[101] γ-Al_2O_3 in the altered B-layer. In the case of the altered A-layer as shown in Fig. 7a, the Mo–Mo distance is about 0.32 nm, which is almost equal to that of MoS_2, 0.316 nm. The lattice misfit is only −2.3%. In this case, however, interplanar spacing meeting at a 30° angle to (20$\bar{2}$) γ-Al_2O_3 should be about 0.16 nm ((110)MoS_2), which differs from the above-mentioned experimental value of 0.25 nm. Therefore, this situation cannot represent our observation. On the other hand, the Mo–Mo distance in the altered B-layer as shown in Fig. 7b is about 0.28 nm, which is about 89% of that of MoS_2, 0.316 nm. The lattice misfit in the altered B-layer is 11%, larger than that in the altered A-layer, −2.3%. In this case, however, the interplanar spacing meeting at a 30° angle to (20$\bar{2}$)γ-Al_2O_3 is about 0.25 nm ((100)MoS_2) which agrees with the above-mentioned experimental value of 0.25 nm.

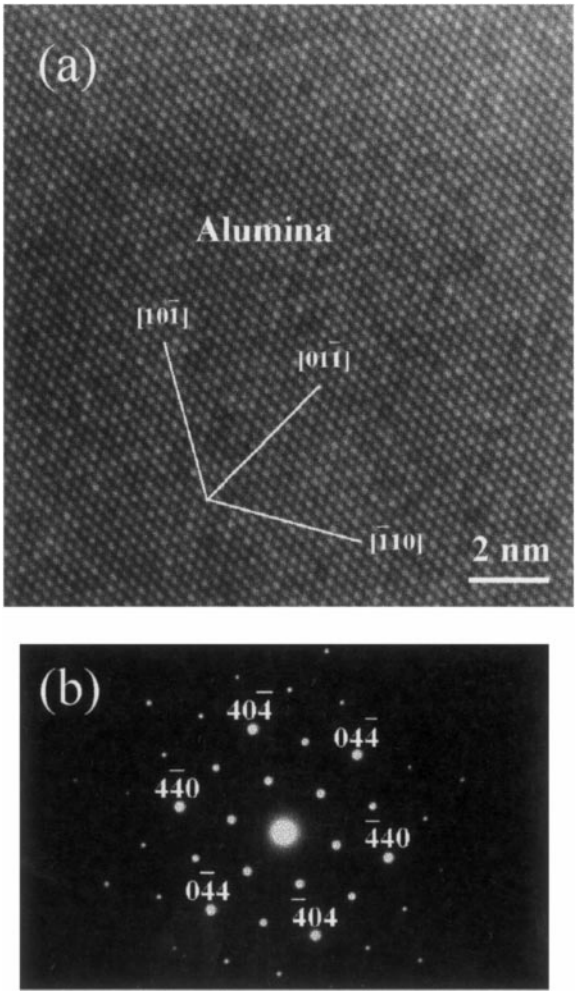

FIG. 5. (a) HREM image of the Mo model catalyst supported on the γ-Al_2O_3/(111) $MgAl_2O_4$ substrate after sulfidation at 573 K. (b) Selected-area diffraction pattern.

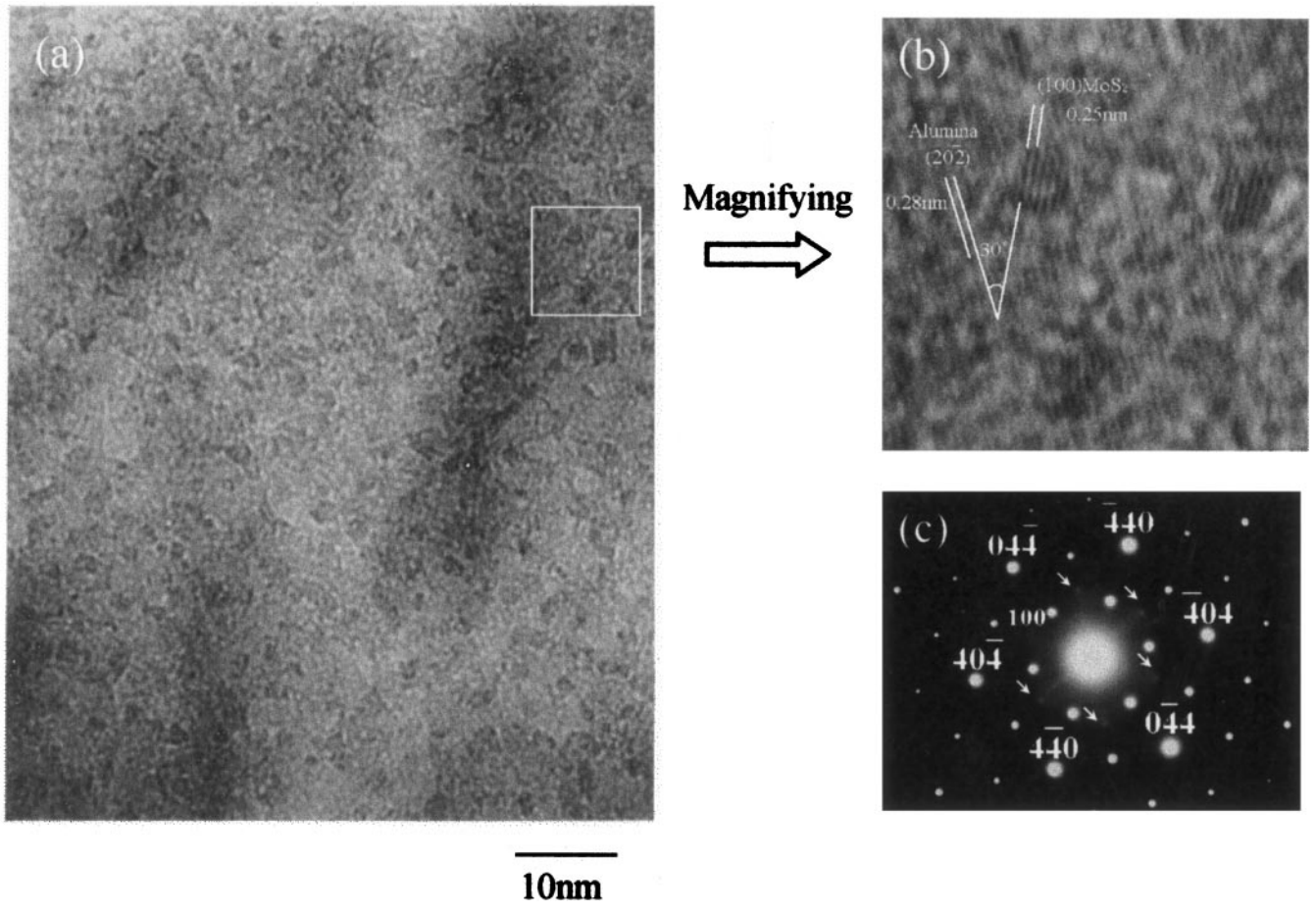

FIG. 6. (a) TEM micrograph of the Mo model catalyst supported on the γ-Al_2O_3/(111) $MgAl_2O_4$ substrate after sulfidation at 773 K. (b) HREM image by increasing the magnification of (a). (c) Selected-area diffraction pattern.

Consequently, not the altered A-layer, but the altered B-layer is considered to represent the cluster–support interface of this Mo model catalyst. The reason for this phenomenon can be explained as follows: in the altered B-layer, all Mo atoms are equivalent in electrical states and are located in the same plane as in MoS_2 (Fig. 2a), whereas all Mo atoms in the altered A-layer are not equivalent. Therefore, the total strain energy of the altered B-layer is thought to be less than that of the altered A-layer. Consequently, the altered B-layer can more frequently appear than the altered A-layer.

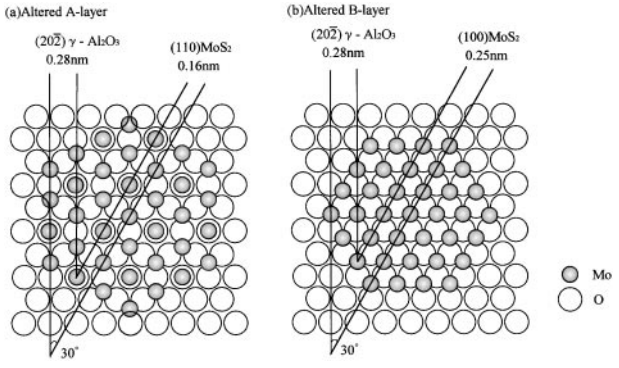

FIG. 7. Schematic drawings of possible cluster–support interface of the Mo model catalyst supported on the γ-Al_2O_3/(111) $MgAl_2O_4$ substrate after sulfidation at 773 K. (a) Altered A-layer, (b) altered B-layer.

Figure 8 shows the particle size distribution of the synthesized particles after sulfidation at 773 K obtained from the TEM micrograph, as shown in Fig. 6a. Approximately 80% of the particles are under 2 nm in diameter. The mean particle size is approximately 1.73 nm, which indicates that a typical particle consists of approximately 37 Mo atoms in one layer as shown in Fig. 7b. In this way, MoS_2 clusters supported on (111) γ-Al_2O_3 have a relatively small size and a narrow size distribution compared with that seen with conventional catalysts (4, 19). The reasons for this phenomenon are considered as follows: the cluster–support interaction of this model catalyst is thought to be stronger than that of conventional catalysts due to the regular surface structure of γ-Al_2O_3 single crystal thin film. Consequently, the above-mentioned lattice misfit between the particles and the film would prevent the particles from growing in diameter.

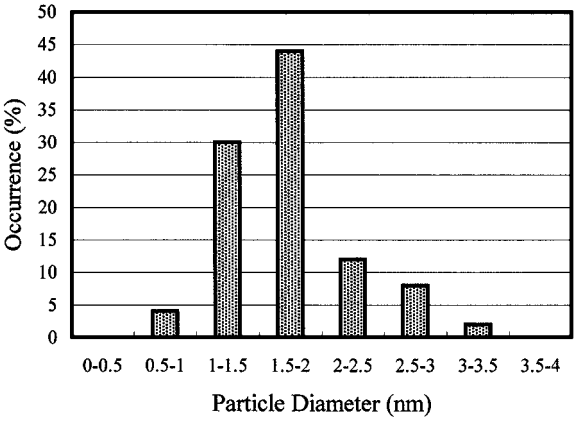

FIG. 8. Particle size distribution of the Mo model catalyst supported on the γ-Al_2O_3/(111) $MgAl_2O_4$ substrate after sulfidation at 773 K, obtained from TEM micrograph as shown in Fig. 6a.

In summary, by using the (111) γ-Al_2O_3 single crystal thin film as a model support, relatively uniform basal-bonded MoS_2 particles could be successfully prepared.

HREM Observation of Mo Model Catalysts Supported on γ-Al_2O_3/(100) $MgAl_2O_4$ Substrates

The TEM micrographs of the Mo model catalyst supported on the γ-Al_2O_3/(100) $MgAl_2O_4$ substrate after MoO_x deposition and oxidation at 673 K have no apparent difference compared with those before deposition, as described in the case of the γ-Al_2O_3/(111) $MgAl_2O_4$ substrate. This HREM observation suggests that MoO_x could be present in highly dispersed form or as amorphous particles.

The TEM micrograph of the Mo model catalyst supported on the γ-Al_2O_3/(100) $MgAl_2O_4$ substrate after sulfidation at 773 K indicates that many small black lines appear. Some are straight; others are curved. By increasing the magnification of the micrograph as shown in Figs. 9a and 9b, the lattice images of the cluster and the alumina film are clearly recognized. Most of the clusters have a single layer, and the others have two or three layers which have approximately 0.6 nm interplanar spacing agreeing with that of bulk (002)MoS_2. Therefore, these clusters are assumed to be edge-bonded to the alumina film. The mean cluster length is approximately 2 nm.

In consideration of the above results, the cluster–support interface of this Mo model catalyst is briefly discussed here. In the same way as (111) γ-Al_2O_3, one possibility is to assume that Al atoms located in octahedral cation positions in (100) γ-Al_2O_3 should be exchanged by Mo atoms, as shown in Fig. 10a. In this case, the arrangement of Mo atoms in Fig. 10a is similar to that in Fig. 2b: compared with the (100) plane of bulk MoS_2 as shown in Fig. 2b, the Mo–Mo distance along the *c* axis is 0.56 nm, which is about 91% shrunken from 0.615 nm, and the Mo–Mo distance perpendicular to the *c* axis is 0.28 nm, which is about 89% shrunken from 0.316 nm. The epitaxial relation is (100)MoS_2//(100) γ-Al_2O_3, [001]MoS_2//[011] γ-Al_2O_3 in this case. If every second Mo atom is eliminated from Fig. 10a (as shown in Fig. 10b), the arrangement of Mo atoms becomes similar to that in Fig. 2c: the Mo–Mo distance along the *c* axis is 0.56 nm, which is about 91% shrunken from 0.615 nm and the Mo–Mo distance perpendicular to the *c* axis is 0.56 nm, which is only 103% extended from 0.547 nm compared with the (110) plane of bulk MoS_2 as shown in Fig. 2c. The

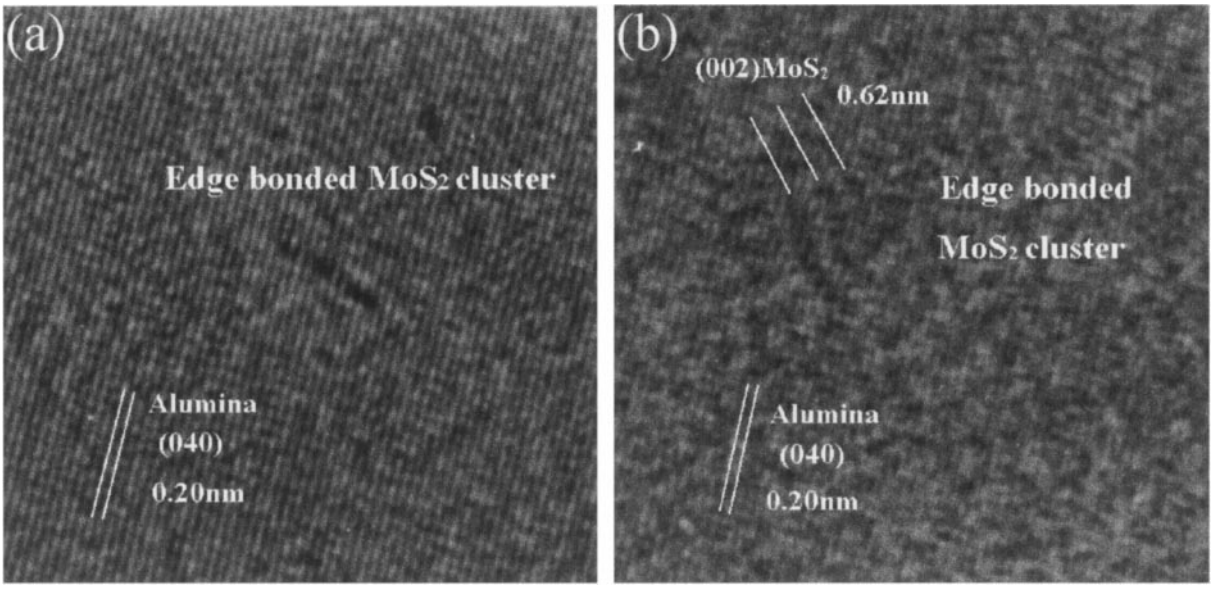

FIG. 9. HREM image of the Mo model catalyst supported on the γ-Al_2O_3/(100) $MgAl_2O_4$ substrate after sulfidation at 773 K. (a) A typical example of the single-layered clusters. (b) An example of the multilayered clusters.

epitaxial relation is (110)MoS_2//(100) γ-Al_2O_3, [001]MoS_2// [011] γ-Al_2O_3 in this case. In this way, approximately 10% of the lattice misfits along *c*-axis in both cases, which forces the MoS_2 clusters compressed, are thought to prevent them from growing stacked along the *c* axis. Consequently, most of the clusters should have a single layer as described above. In addition, since the misfit of the Mo–Mo distance perpendicular to the *c* axis in Fig. 10b is less than that in Fig. 10a, the (110) plane bonding is assumed to appear more frequently than the (100) plane bonding. Anyhow, it must be noted that the lattice misfits in both the (100) plane bonding and the (110) plane bonding lead the clusters to have nonnegligible distortions. For this reason, the clusters should be forced to have curvatures in order to release the strain energy.

Orientation of MoS_2 Clusters on γ-Al_2O_3 Supports

Until now, quite a few discussions about orientations of MoS_2 clusters on γ-Al_2O_3 supports have been carried out using TEM techniques. For example, Pratt *et al.* reported that MoS_2 was present as flakes up to five layers thick, sitting vertically on γ-Al_2O_3 supports (20). However, Srinivasan *et al.* pointed out the difficulties in distinguishing edge bonding from basal bonding because of the artifacts associated with porous structure of the conventional supports (21). By using alumina thin films as model supports, Hayden *et al.* insisted that MoS_2 crystallites were present as hexagonally shaped slabs and bonded with their edge planes to the alumina surface (10). However, their insistence on the existence of edge bonding was denied by Stockmann *et al.* (22) because micropores in their alumina films resulted in the misunderstanding of the distinction of edge bonding from basal bonding. Stockmann *et al*. concluded that MoS_2 particles were only basal bonded, judging from their experimental results. In this way, there is insufficient evidence to show the existence of edge bonding, whereas the existence of basal bonding is generally accepted.

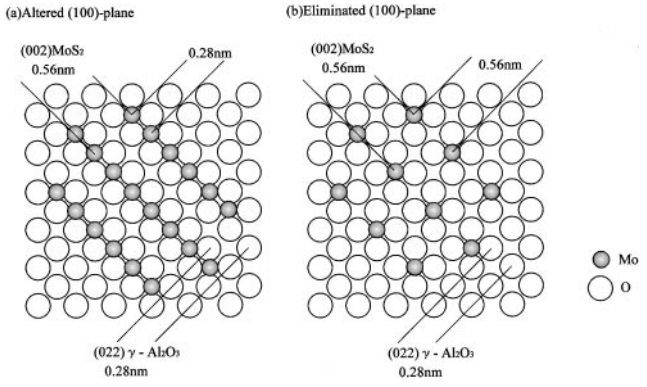

FIG. 10. Schematic drawings of possible cluster–support interface of the Mo model catalyst supported on the γ-Al_2O_3/(100) $MgAl_2O_4$ substrate after sulfidation at 773 K. (a) Altered (100) plane, (b) eliminated (100) plane.

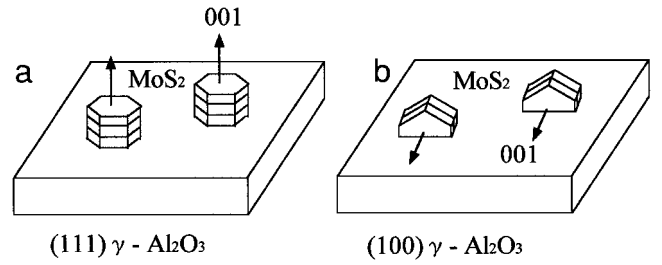

FIG. 11. Effect of surface orientations of γ-Al_2O_3 supports on microstructures of MoS_2 clusters obtained from the present study. (a) Basal-bonded clusters on the (111)γ-Al_2O_3 surface, (b) edge-bonded clusters on the (100) γ-Al_2O_3 surface.

From our experimental results described above, we found that edge-bonded clusters were grown on the (100) γ-Al_2O_3 thin films, while basal bonded clusters were grown on the (111) γ-Al_2O_3 thin films. Since our γ-Al_2O_3 single crystal thin films do not have micropores, it seems reasonable to say that edge bonded clusters are really grown on our (100) γ-Al_2O_3 thin films.

In addition, the present study suggests that important factors for determining orientations of MoS_2 clusters on γ-Al_2O_3 supports could be the similarities between the arrangement of Mo atoms in MoS_2 and the arrangement of Al or O atoms in the γ-Al_2O_3 surface, as described above. A simple explanation can be as follows: the arrangement of Mo atoms in an MoS_2 basal plane has six symmetry axes, agreeing with the (111) γ-Al_2O_3 plane. Therefore, basal bonded clusters are grown on the (111) γ-Al_2O_3 surface. On the other hand, the arrangement of Mo atoms in MoS_2 edge plane has four symmetry axes, agreeing with the (100) γ-Al_2O_3 plane. Therefore, edge bonded clusters are grown on the (100) γ-Al_2O_3 surface. The effect of surface orientations of γ-Al_2O_3 supports on microstructures of MoS_2 clusters described above can be summarized in Fig. 11.

In conclusion, by using γ-Al_2O_3 single crystal thin films with two kinds of surface orientations, it is newly found that the orientation of MoS_2 clusters can be controlled by the surface orientation of supports. The sulfidation mechanism of these model catalysts using XPS analysis will be discussed elsewhere. The activities of these model catalysts are worth further study.

SUMMARY

(i) By using the electron beam evaporation method, epitaxial γ-Al_2O_3 single crystal thin films with a smooth surface were successfully grown on (100) and (111) $MgAl_2O_4$ substrates. The epitaxial relations were (100) γ-Al_2O_3//(100) $MgAl_2O_4$, [010] γ-Al_2O_3//[010] $MgAl_2O_4$ and (111) γ-Al_2O_3//(111) $MgAl_2O_4$, [101] γ-Al_2O_3//[101] $MgAl_2O_4$, respectively.

(ii) Relatively uniform basal bonded clusters were grown on (111) γ-Al_2O_3 thin films. Their particle size

distribution is relatively narrow because of some cluster–support interaction. Their mean particle size was approximately 1.73 nm. The epitaxial relation is thought to be (001)MoS_2//(111) γ-Al_2O_3 and [110]MoS_2//[101] γ-Al_2O_3.

(iii) It was newly found that edge bonded clusters were grown on (100) γ-Al_2O_3 thin films. The mean cluster length was approximately 2 nm. The epitaxial relation is thought to be (110)MoS_2//(100) γ-Al_2O_3, [001]MoS_2//[011] γ-Al_2O_3.

(iv) The present study suggests that important factors to determine the orientations of MoS_2 clusters on γ-Al_2O_3 supports could be the similarities between the arrangement of Mo atoms in MoS_2 and the arrangement of Al or O atoms in the γ-Al_2O_3 surface.

ACKNOWLEDGMENTS

This work has been carried out as a research project of the Petroleum Energy Center and was subsidized by the Ministry of International Trade and Industry.

REFERENCES

1. Topsoe, H., Clausen, B. S., and Massoth, F. E., "Hydrotreating Catalysis." Springer-Verlag, Berlin, 1996.
2. Prins, R., de Beer, V. H. J., and Somorjai, G. A., *Catal. Rev. Sci. Eng.* **31**, 1 (1989).
3. Eijsbouts, S., Heinerman, J. J. L., and Elzerman, H. J. W., *Appl. Catal. A* **105**, 53 (1993).
4. Vrinat, M., Breysse, M., Geantet, C., Ramirez, J., and Massoth, F., *Catal. Lett.* **26**, 25 (1994).
5. Daage, M., and Murray, H. H., *Prepr. Am. Chem. Soc. Div. Pet. Chem.* **38**, 660 (1993).
6. Daage, M., and Chianelli, R. R., *J. Catal.* **149**, 414 (1994).
7. Schoofs, G. R., Preston, R. E., and Benziger, J. B., *Langmuir* **1**, 313 (1985).
8. Gellman, A. J., Neiman, D., and Somorjai, G. A., *J. Catal.* **107**, 92 (1987).
9. Takata, Y., Yokoyama, T., Yagi, S., Happo, N., Sato, H., Seki, K., Ohta, T., Kitajima, Y., and Kuroda, H., *Surf. Sci.* **259**, 266 (1991).
10. Hayden, T. F., and Dumesic, J. A., *J. Catal.* **103**, 366 (1987).
11. Mcintyre, N. S., and Chan, T. C., and Spevack, P. A., *Appl. Catal.* **63**, 391 (1990).
12. Diemann, E., Weber, Th., and Muller, A., *J. Catal.* **148**, 288 (1994).
13. Muijsers, J. C., Weber, Th., van Hardeveld, R. M., Zandbergen, H. W., and Niemantsverdriet, J. W., *J. Catal* **157**, 698 (1995).
14. De Jong, A. M., de Beer, V. H. J., van Veen, J. A. R., and Niemantsverdriet, J. W., *J. Vac. Sci. Technol. A* **15**, 1592 (1997).
15. Josek, K., Linsmeier, Ch., Knozinger, H., and Taglauer, E., *Nucl. Instr. Methods Phys. Res. B* **64**, 596 (1992).
16. Sakashita, Y., Aoki, N., and Yoneda, T., *Sci. & Tech. in Catal.* **1998**, 403 (1998).
17. Schuit, G. C. A., and Gates, B. C., *AIChE J.* **19**, 417 (1973).
18. Knozinger, H., and Ratnasamy, P., *Catal. Rev. Sci. Eng.* **17**, 31 (1978).
19. Ramirez, J., Fuentes, S., Diaz, G., Vrinat, M., Breysse, M., and Lacroix, M., *Appl. Catal.* **52**, 211 (1989).
20. Pratt, K. C., Sanders, J. V., and Christov, V., *J. Catal.* **124**, 416 (1990).
21. Srinivasan, S., Datye, A. K., and Peden, C. H. F., *J. Catal.* **137**, 513 (1992).
22. Stockmann, R. M., Zandbergen, H. W., van Langeveld, A. D., and Moulijn, J. A., *J. Mol. Catal. A* **102**, 147 (1995).